IMEKO 24th TC3, 14th TC5, 6th TC16 and 5th TC22 International Conference
11 – 13 October 2022, Cavtat-Dubrovnik, Croatia

ABSOLUTE TIME-BASED DYNAMIC MULTI-SENSOR CALIBRATION FOR MEMS ACCELEROMETERS – A CONCEPT STUDY

B. Seeger[1], Th. Bruns[2]

Physikalisch Technische Bundesanstalt, Braunschweig, Germany,
[1] benedikt.seeger@ptb.de, [2] thomas.bruns@ptb.de

Abstract:
This paper describes an absolute time-based concept to simultaneously calibrate a large number of MEMS sensors using Ethernet as communication interface and investigates new uncertainty influences related to the absolute time base.

Keywords: Multi-sensor calibration; MEMS; accelerometer; absolute time; dynamic calibration

1. INTRODUCTION

Recently, some dynamic calibration procedures for accelerometers with digital output have been developed [1], [2], [3]. The acquisition of the statistical parameters of the transfer functions of MEMS sensors is of great interest [4]. For this purpose, many sensors need to be calibrated, preferably simultaneously in the same system. If both the reference and the DUT (device under test) signals are acquired in relation to an absolute time base, the phase relationship of the signals can be determined without any further synchronisation of the sampling. In this way, any number of DUT signals can be acquired simultaneously with independent low-cost devices.
In contrast to a calibration according to ISO 16063-11, the uncorrelated jitter and drift of the different time bases lead to an additional uncertainty component using this new concept of calibration.

2. DATA AQUSITION

As part of the European Met4FoF research project within the EMPIR programme [5], an open-source microcontroller-based data acquisition unit (DAU) was developed that reads MEMS sensors with digital output and sends the measurement data with associated absolute timestamps (with nanosecond resolution and uncertainty awareness) via a state-less data and description protocol using UDP (User Datagram Protocol) [6] to a receiving PC. UDP is part of the Internet Protocol Suite, hence, this inexpensive proven technology for the connection of many devices is readily available at large scale. Figure 1 shows the proposed setup for the sensor data acquisition for 16 3-axis-sensors. Groups of four sensors are connected to a DAU which acquires the data as sets of x, y, and z-acceleration values and forwards them after timestamping and conversion from integer readings to SI units to a server that stores the measured values, timestamps and metadata in an HDF5 file for post processing.

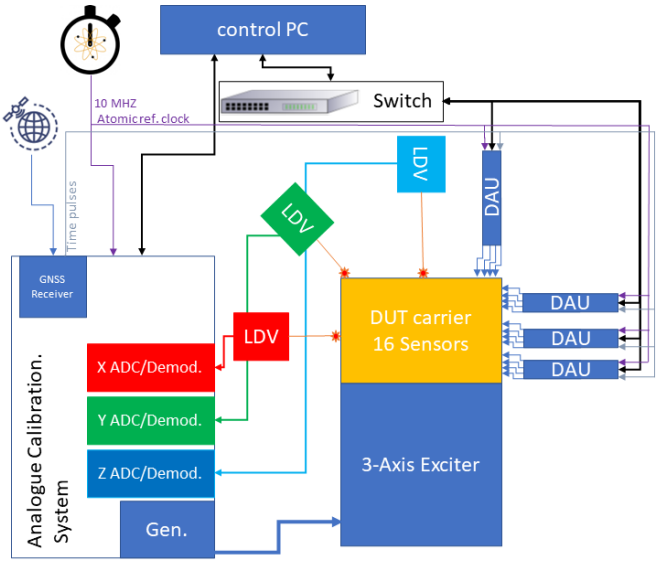

Figure 1: Proposed 3-axis multi-sensor calibration system

3. TRANSFER FUNCTION

The MEMS sensors generate their sample clock internally and therefore the measured values carry the timestamps $t_{\mathrm{DUT0}\,0}, t_{\mathrm{DUT0}\,1}, \ldots, t_{\mathrm{DUT0}\,n_{\mathrm{DUT0}}}$ for the first sensor and $t_{\mathrm{DUT1}\,0}, t_{\mathrm{DUT1}\,1}, \ldots\ t_{DUT1\,n_{\mathrm{DUT1}}}$ for the second, and so on. Since the sampling frequencies of the sensors are slightly different and vary with time, the number of samples n_{DUT} in an observation window may differ.

The integer (int64) absolute timestamps in nanoseconds elapsed since January 1st, 1970, 00:00:00 UTC – the Unix epoch, currently have 61 bits of significant data, consequently there is a loss of precision if they are directly converted to floating point (f64) numbers. The absolute timestamps are therefore converted to relative timestamps for the subsequent IEEE 1057 conformant three-parameter

sine approximation. As a reference point, the timestamp of the first reference sample can be used. The relative timestamps are calculated as follows:

$$\Delta_{\mathrm{DUT0}\,n} = t_{\mathrm{DUT\,0}\,n} - t_{\mathrm{REF\,0}}$$
$$\Delta_{\mathrm{DUT1}\,n} = t_{\mathrm{DUT1}\;n} - t_{\mathrm{REF\,0}}\,. \quad (1)$$

Note that the relative timestamps do not need to be all positive and that a loss of precision occurs due to mantissa overflow in the subsequent conversion to a 64-bit floating-point value about 87 hours (2^{48} ns) after the relative time start.

By means of a three-parameter sine approximation (3PSA) based on relative timestamps, amplitude $\hat{a}(\omega)$ and initial phase $\varphi(\omega)$ are determined with respect to $t_{\mathrm{REF\,0}}$ for all signals, including the reference. The magnitude and phase response of the complex transfer function is subsequently calculated as follows:

$$|S(\omega)| = \frac{\hat{a}_{\mathrm{DAU}}(\omega)}{\hat{a}_{\mathrm{REF}}(\omega)}$$
$$\varphi(\omega) = \varphi_{\mathrm{DAU}}(\omega) - \varphi_{\mathrm{REF}}(\omega)\,. \quad (2)$$

Figure 2 shows a simulation of non-equidistant sampling of a 400 Hz sine signal by four digital sensors and the analogue calibration system, signal parameters are given in Table 1 shows a simulation of four digital sensors sampling a 400 Hz sine signal with a nominal sampling frequency of 1 kHz as well as the reference signal sampled uniformly by the analogue calibration system with a sampling frequency of 10 kHz. The absolute timestamps were converted to relative timestamps in respect to the first reference sample.

The sampled timestamps differ due to the variation of the sample frequency of the different sensors; the fourth sensor DUT3 has a sample with a negative timestamp.

To simulate a non-equidistant sampling, normally distributed phase noise was added to the sampling time points. The simulation parameters are given in the following table.

Table 1: Simulation parameters of the sensor sampling simulation shown in Figure 2.

Sensor	Mean sampling frequency f_s	Initial sampling phase	Sampling jitter std. dev.
Unit	Hz	°	% of $1/f_s$
DUT0	1000	0	15
DUT1	950	20	11
DUT2	1050	80	8
DUT3	1025	-30	3

In the figure, the data points shown as filled dots are given with absolute timestamps. The triangles show data points with normally distributed jitter but corrected sampling frequency. The correction can be done either by timestamping (as in this work), by a four-parameter sine approximation [7] or via period-length measurement [7]. The crosses show values where the nominal sampling frequency was assumed. After a short measurement time, a substantial time difference between nominal and actual sample time occurs, and a three-parameter sine approximation (3PSA) would no longer yield reasonable values.

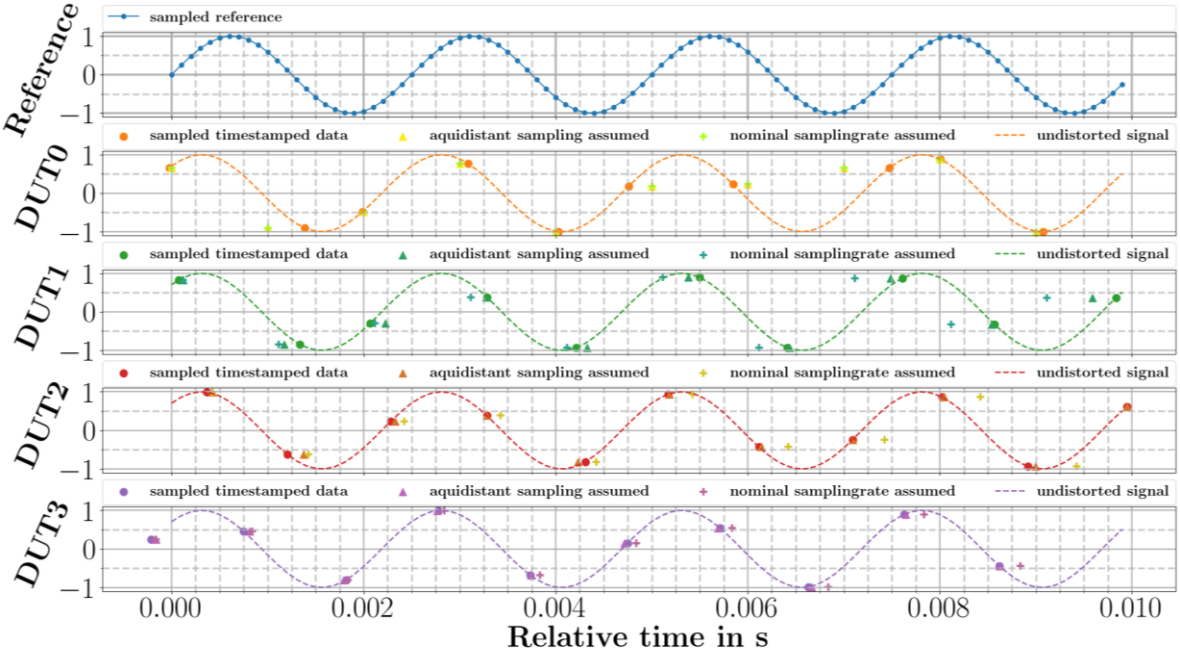

Figure 2: Simulation of non-equidistant sampling of a 400 Hz sine signal by four digital sensors and the analogue calibration system, signal parameters are given in Table 1

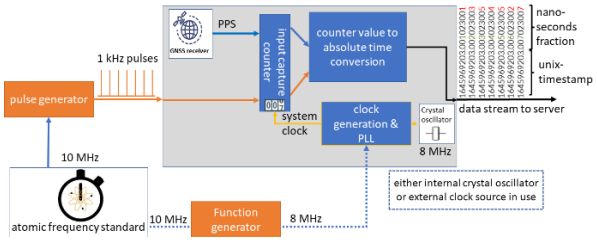

Figure 3: Absolute timestamping test setup

Drift and jitter cause a deviation of the absolute timestamps since different time bases are used for the reference and each DAU. These effects are no longer negligible in the calculation of the transfer function due to their statistical independence.

To investigate this influence, a data ready signal (DRS) was mimicked by a (rectangular) 1 kHz waveform, which was derived from PTB's central frequency distribution. This DRS was timestamped by two DAUs each using its individual GPS-controlled oscillator. Based on the timestamps of the latter and the presumption that the DRS represented an ideal time course (ITC), the continuous deviation $\Delta t_{\mathrm{ITC}}(t)$ was determined. A schematic of the setup is shown in Figure 3.

Figure 4 shows in purple and blue the time deviations from the expected values for two boards with internal 8 MHz oscillator as clock source and two different GNSS (Global Navigation Satellite Systems) modules. The difference between these time deviations is shown in green. Only a small correlation of the deviations could be found. The sawtooth-shaped artifacts within each curve are characteristic for the internal clock of the STM32 Nucleo board.

The orange and brown plots show the deviations of the timestamps using a single common GNSS for both DAUs (DRS source unchanged). The time deviations for this case are almost entirely attributable to the GNSS module and they are therefore strongly correlated. The time difference between the modules shown in red is in the range of the quantisation limit of 9.25 ns.

4.1. Time deviations and phase noise

If a dynamic signal is sampled with a sample pulse, the signal's representation in the frequency domain is always convolved with the Fourier transform of the sample clock. Therefore, the temporal behaviour of the sampling signal, i.e. its jitter or its spectral representation, the phase noise, is of interest. Figure 5 is taken from a recommended article [8] on jitter and phase noise that visualises this convolution; [9] also provides a good overview of this topic.

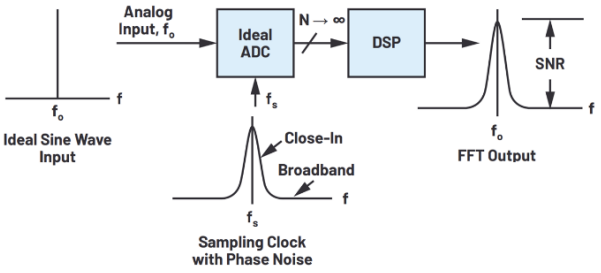

Figure 5: Effect of phase noise on the sampling of an ideal sine, modified from [8]

The deviations of the timestamps from ITC correspond to a phase noise that can be characterised by the following method if one can assume that the jitter of the mimicked 1 kHz DR signal is small compared to the uncertainty of the timestamps.

For $n = 2^{20}$ consecutive timestamps $t_0, t_1 \ldots t_n$, the function value of a sinusoidal oscillation with the DR signal frequency f_s, in our case 1 kHz, an amplitude of 1 and zero initial phase, is generated. If the formerly determined deviations $\Delta t_{\mathrm{ITC}}(t)$ are added to the simulated (perfect) timestamps prior to the calculation of the sine, a deviation in the sample amplitude of the generated signal occurs, and it becomes noisy. The Fourier transform of this signal directly provides the phase noise of the timestamping as follows:

$$\mathrm{Phasenoise}(f) = \mathcal{F}(1 \cdot \sin(f_s \cdot 2\pi \cdot t\,))/n\,. \quad (3)$$

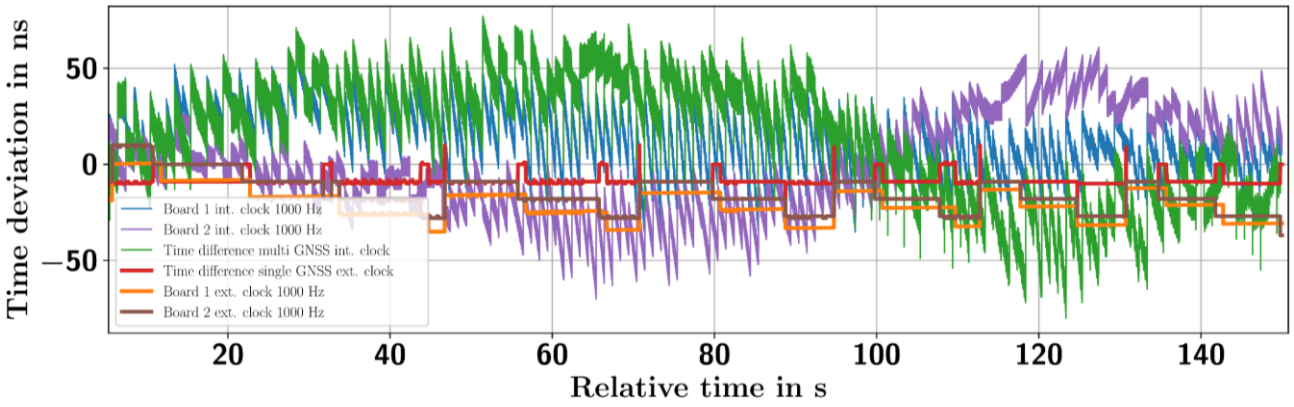

Figure 4: Time deviations for two DAUs in two configurations, as well as the difference of the timestamps

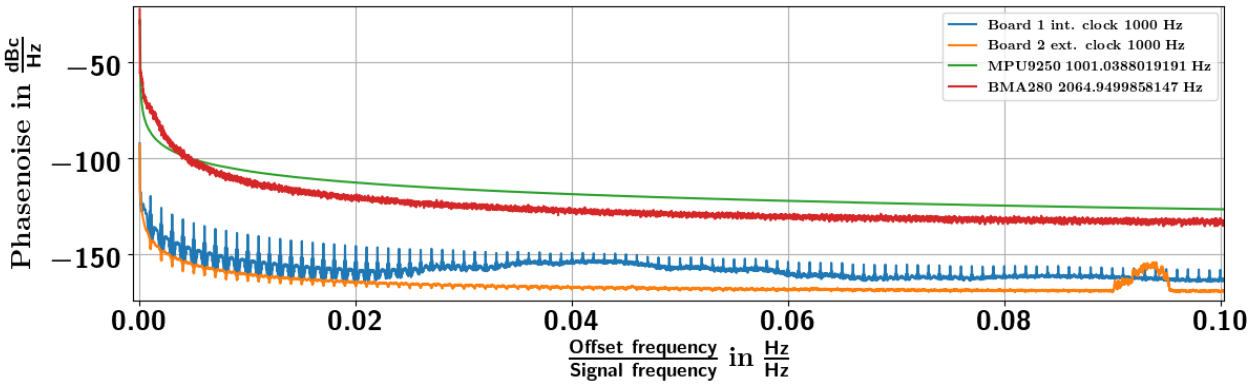

Figure 6: Calculated phase noise for boards with internal oscillator (blue) and external normal frequency clock source (orange), as well as measured phase noise of two digital MEMS accelerometers

It should be taken into account that the effect of phase noise on a signal is proportional to the signal frequency. Figure 6 shows in blue the phase noise determined by this method for the use of the internal GNSS-controlled oscillator of a DAU. There are periodic spikes occurring with a multiple of 1 Hz which are caused by the resynchronisation of the oscillator frequency with the GNSS time pulses every second.

Even if a very stable clock source is used, the periodic synchronisation effects are noticeable (orange), which are caused by the jitter of the GNSS pulses and could be reduced by suitable algorithms in the DAU.

The same methodology can be used to study the phase noise of digital sensors without any external clock information. For this purpose, a sufficiently long data set of e.g. $n = 2^{20}$ samples is recorded. The average sampling frequency is determined by the following equation:

$$f_s = (t_n - t_0)/n\,. \tag{4}$$

With this sampling frequency, the phase noise can be directly determined from the resulting timestamps (which are presumed to be strictly periodic) according to (2).

In Figure 6 is shown as well as the measured phase noise of two digital sensors: A *Bosch BMA280* (red), which has significant narrow-band phase noise in the range up to about $0.05\frac{\Delta f}{f_c} = \frac{10\text{ Hz}}{2064\text{ Hz}}$ and a *TDK Invensense MPU9250,* which demonstrates significantly less narrow-band phase noise, probably due to an internal temperature compensation in the PLL that generates the sampling clock of the latter sensor.

4.2. Sine approximation simulations

Jitter leads to a reduction of the measured amplitude and a deviation of the measured phase [9]. To investigate both the amplitude reduction and the phase deviation due to timestamping jitter, three-parameter sine approximations using absolute timestamps and further Monte Carlo experiments have been performed.

For each of the 200 simulations per frequency point, 10000 consecutive timestamps were generated either from the real time deviations or the timestamps with normally distributed jitter. For these timestamps, a sinusoidal oscillation was then generated with the test frequency, amplitude 1.0 and initial phase of zero.

The simulated frequencies are in the range up to 50 kHz. All frequencies above 500 Hz are subsampled since the simulated sampling clock is 1 kHz.

Frequencies violating the Nyquist-Shannon sampling theorem for under-sampling were shifted by +10 Hz.

The amplitude, phase and DC offset are determined from these synthesised signals by a 3PSA.

Figure 7 visualizes the mean values of the fitted amplitudes divided by the nominal amplitude. For the normally distributed jitter, a Gaussian-shaped amplitude decrease over frequency can be observed. The cut-off frequency correlates negatively with the square of the jitter amplitude.

Since the normally distributed jitter is uncorrelated in time, this behaviour can be explained by a convolution of the Dirac-shaped sample pulse with the Gaussian-shaped probability density function of the jitter. The Fourier-transformed Gaussian signals are themselves also Gaussian.

For the real jitter, the amplitude decrease is at least one order of magnitude smaller because of the temporal correlation of the sample jitter.

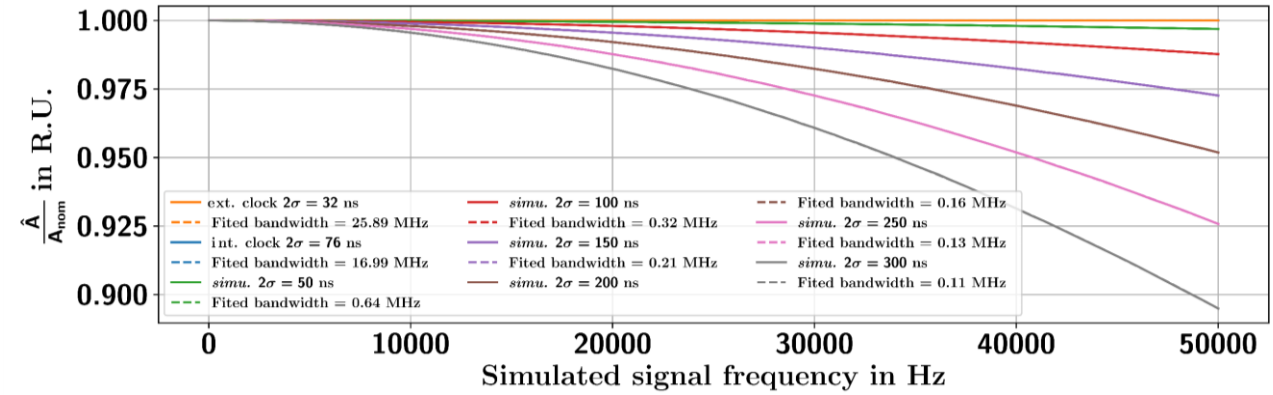

Figure 7: Amplitude reduction by sample jitter and fitted cut-off frequencies

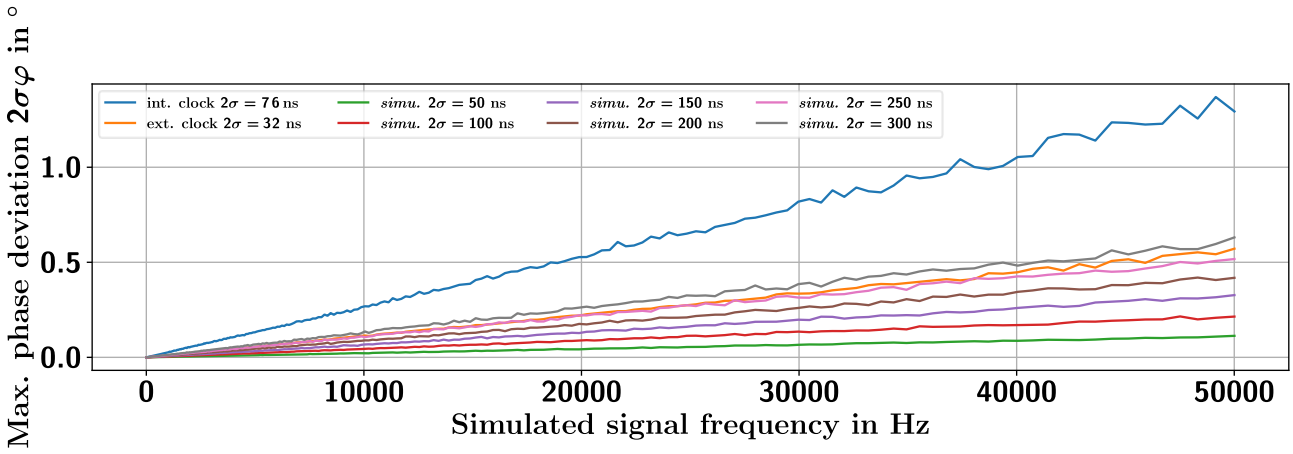

Figure 8: Statistical deviation of the simulated phase values for real and simulated jitter

Since the jitter is unbiased, there is no deviation of the phase mean. In contrast to the amplitude calculations, the standard deviation of the simulated phases is significantly worse (see Figure 8 orange and blue) than the linear jitter amplitude /phase uncertainty relationship of the normally distributed values would suggest. This is mainly due to the low frequency drift components of the real sample time deviations.

4.3. Use of common time and clock source

By using a sufficiently good clock source and a common absolute time source, e. g., a single, common GNSS module, this uncertainty influence can be almost completely avoided. See Figure 4, where the red graph shows the difference between the timestamps of two different DAUs with the same clock source and absolute time source but independent internal PLLs. In this setup, the time quantisation is dominant and results in a phase uncertainty from this source of about 0.1° for a frequency of 50 kHz.

5. SUMMARY

We present a method based on absolute timestamps for the simultaneous calibration of a large number of digital accelerometers. A sinusoidal vibration is excited and recorded by all sensors including the reference. An arbitrary reference point in time is selected relative to this, sine approximations are performed, and the complex transfer coefficients are calculated. The use of different time bases results in new uncertainty influences which are investigated and quantified based on simulations and experiments. Due to the temporal correlation of the real jitter, simulations or calculations with normally distributed jitter are not sufficient and a Monte Carlo simulation is necessary. The temporal correlation of the jitter usually leads to an improvement of the amplitude calculation and a deterioration of the phase determination compared to the normally distributed case. It could be demonstrated that a single common clock and time source should be used if possible.

6. REFERENCES

[1] B, Seeger, Th. Bruns, Primary calibration of mechanical sensors with digital output for dynamic applications, Acta IMEKO 10 (2021) 3, pp. 177-184.
DOI: 10.21014/acta_imeko.v10i3.1075

[2] Shimoda T, Kokuyama W, Nozato H, Primary calibration system for digital accelerometers,

Metrologia 58 045002, 2021.
DOI: 10.1088/1681-7575/ac0403

[3] A. Prato, F. Mazzoleni, A. Schiavi, Traceability of digital 3-axis MEMS accelerometer: simultaneous determination of main and transverse sensitivities in the frequency domain, Metrologia, vol. 57, no. 3.
DOI: 10.1088/1681-7575/ab79be

[4] A. Prato, F. Mazzoleni, F. R. Pennecchi, G. Genta, M. Galetto, A. Schiavi, Towards large-scale calibrations: a statistical analysis on 100 digital 3-axis MEMS accelerometers, IEEE Int. Workshop on Metrology for Industry 4.0 & IoT (MetroInd4.0&IoT), Rome, Italy, 07-09 June 2021, pp. 578-582.
DOI: 10.1109/MetroInd4.0IoT51437.2021.9488465

[5] Metrology for the Factory of the Future (17IND12 - Met4FoF) project homepage. Online [Accessed 20221209]
https://www.ptb.de/empir2018/met4fof

[6] S. Eichstädt, M. Gruber, A. P. Vedurmudi, B. Seeger, Th. Bruns, G. Kok, Toward Smart Traceability for Digital Sensors and the Industrial Internet of Things, Sensors. 2021; 21(6):2019.
DOI: 10.3390/s21062019

[7] G. D'Emilia, A. Gaspari, E. Natale, A. Prato, F. Mazzoleni, A. Schiavi, Managing the sampling rate variability of digital MEMS accelerometers in dynamic calibration, IEEE Int. Workshop on Metrology for Industry 4.0 & IoT (MetroInd4.0&IoT), Rome, Italy, 07-09 June 2021, pp. 687-692.
DOI: 10.1109/MetroInd4.0IoT51437.2021.9488520

[8] L. Paculanan, J. N. Garlitos, The Easy Steps to Calculate Sampling Clock Jitter for Isolated, Precision High Speed DAQs, analog-dialogue, 2021, vol. 55, no. 4. Online [Accessed 20221209]
https://www.analog.com/media/en/analog-dialogue/volume-55/number-4/the-easy-steps-to-calculate-sampling-clock-jitter-for-isolated-precision-high-speed-daqs.pdf

[9] C. A.-Leme, Clock Jitter Effects on Sampling: A Tutorial, IEEE Circuits and Systems Magazine, vol. 11, no. 3, 2011.
DOI: 10.1109/MCAS.2011.942067